

Raman spectroscopic evidence of impurity-induced structural distortion in SmB_6

Thi Huyen Nguyen¹ | Thi Minh Hien Nguyen^{1,2} | Boyoun Kang³ | Beongki Cho³ |
Mancheon Han⁴ | Hyoung Joon Choi⁴ | Mihye Kong⁵ | Yongjae Lee⁵ | In-Sang Yang¹ 

¹Department of Physics, Ewha Womans University, Seoul, Korea

²Institute of Physics, Vietnam Academy of Science and Technology, Hanoi, Vietnam

³School of Materials Science and Engineering, Gwangju Institute of Science and Technology (GIST), Gwangju, Korea

⁴Department of Physics, Yonsei University, Seoul, Korea

⁵Department of Earth System Sciences, Yonsei University, Seoul, Korea

Correspondence

In-Sang Yang, Department of Physics, Ewha Womans University, Seoul, Korea.
Email: yang@ewha.ac.kr

Present Address

Thi Huyen Nguyen, Center for Correlated Electron Systems (CCES), Institute for Basic Science (IBS), Seoul 08826, Korea; or Department of Physics and Astronomy, Seoul National University, Seoul 08826, Korea.

Funding information

KISTI Supercomputing Center, Grant/Award Number: KSC-2016-C3-0006; National Research Foundation of Korea, Grant/Award Numbers: 2011-0018306, 2017R1A2B2008538, 2018R1A3B1052042, No. 2017R1A2B2009309

Abstract

Impurity-induced structural distortion in SmB_6 is suggested by Raman spectroscopy study on impurity-controlled samples. Significant differences in the Raman spectra of single crystals $\text{SmB}_6(6\text{N})$, synthesized with 99.9999%-pure boron, and $\text{SmB}_6(3\text{N})$, synthesized with 99.9%-pure boron, are detected. While no noticeable differences are detected in the X-ray diffraction of $\text{SmB}_6(3\text{N})$ and $\text{SmB}_6(6\text{N})$, all the Raman phonon modes of the T_{2g} , E_g , and A_{1g} of $\text{SmB}_6(3\text{N})$ are clearly broader and shift to higher wavenumbers than those of $\text{SmB}_6(6\text{N})$, and the T_{2g} and E_g modes of $\text{SmB}_6(3\text{N})$ show doublet features. Based on the high-pressure Raman measurements and phonon calculation in uniaxial compression model, we argue that small amount of impurities in $\text{SmB}_6(3\text{N})$ is enough to induce anisotropic distortion in the B_6 octahedra, leading to peculiar behaviors in Raman spectrum of $\text{SmB}_6(3\text{N})$. Our results may present a clue for understanding the current puzzles about SmB_6 of various origins with different impurities.

KEYWORDS

line broadening, octahedral distortion, Raman upshift, SmB_6 , structural distortion

Thi Huyen Nguyen, Center for Correlated Electron Systems (CCES), Institute for Basic Science (IBS), Seoul 08826, Korea
; or Department of Physics and Astronomy, Seoul National University, Seoul 08826, Korea.

1 | INTRODUCTION

Although it has been widely studied for several decades, SmB_6 remains one of the most puzzling materials in the research community. While it is generally believed to be

This is an open access article under the terms of the Creative Commons Attribution-NonCommercial License, which permits use, distribution and reproduction in any medium, provided the original work is properly cited and is not used for commercial purposes.

© 2019 The Authors. Journal of Raman Spectroscopy published by John Wiley & Sons Ltd

a narrow-gap insulator due to the hybridization of *d*-electrons with *f*-electrons in Sm ions, SmB₆ has two contradictory features: a gapless metallic character and a narrow-gap insulator character.^[1–4] Topological Kondo insulator with a metallic surface state provides a compromise for these contradictions.^[5,6] However, the same measurements performed by two different groups, that is, evaluation of the de Haas van Alphen effects on SmB₆, led to two radically different interpretations of two-dimensional electron orbits^[7] and a three-dimensional Fermi surface^[8] in SmB₆. Some experiments support the two-dimensional nature of the electronic state,^[4,9] whereas others support the three-dimensional electronic states.^[10–12] In addition, in Angle-Resolved Photoemission Spectroscopy studies on SmB₆, Neupane et al.^[9] reported that the surface state exists below 30 K inside the hybridization gap. On the other hand, Xu^[13] and Jiang et al.^[14] claimed that the surface state can be found in a wide temperature range from 50 to 110 K or even 150 K. The origin of the metallic state of SmB₆ is still unresolved.

The cubic structure of SmB₆ belongs to the space group O_h^1-Pm3m , and group theoretical analysis shows that the Γ -point phonon modes are distributed among irreducible representation as follows: $\Gamma = A_{1g} + E_g + T_{2g} + T_{1g} + 3T_{1u} + T_{2u}$. Among these, $A_{1g} + E_g + T_{2g}$ are Raman active. The Raman spectra of SmB₆ have been investigated by several groups.^[15–17] Nyhus et al.^[15] observed a gap formation in their electronic scattering spectra of SmB₆ below 70 K. Valentine et al.^[16] investigated the effects of Sm vacancies on the gap and found that the presence of even 1% of Sm vacancies lead to suppression of the hybridization gap. The line shapes and vibration frequency of the phonons of RB₆ were found to strongly depend on the valence of *R* ions. For instance, the T_{2g} mode is asymmetric for the trivalent *R* but symmetric for the divalent *R*. Likewise, the E_g mode is a broad single peak for trivalent and a doublet for divalent *R*.^[17,18] However, previous Raman studies on CaB₆ and EuB₆ show the line shapes or number of peak components of each phonon mode are not related to the valence of *R* ion.^[19,20]

In principle, physical properties of a material are strongly dependent on its crystal symmetry. Neutron scattering and X-ray diffraction (XRD) are usually useful to characterize crystal symmetry and structural distortion. However, neutron scattering is not applicable for the substances which contain strong neutron absorber atoms, such as ¹⁴⁹Sm and ¹⁰B in SmB₆. In addition, slight change in symmetry in RB₆ (*R* = Ca, rare earths) could be also difficult to detect using XRD. This is partly due to the fact that the XRD scattering is not sensitive to light element such as B (*Z* = 5) atom compared with

heavier *R* ions. Consequently, a subtle change of the direction of the B octahedra in RB₆ may not be detected by XRD. Raman scattering, on the other hand, is very sensitive to changes in the force constant resulting from slight distortion of the structure, leading to a significant change in the Raman spectra. Indeed, our previous Raman studies on CaB₆^[19] and Eu_{1-x}La_xB₆^[20] showed that the phonon wavenumbers and the line shape depend strongly on impurities or doping, whereas their XRD showed no noticeable differences. Interestingly, some physical properties, such as the resistivity and magnetism of hexaborides, for example, CaB₆, are known to depend on the impurities in the B ingredients.^[21,22] For the CaB₆(6N) and CaB₆(3N) single crystals synthesized with 99.9999%-pure B₆ and 99.9%-pure B, respectively, Cho et al.^[22] reported that ferromagnetism (FM) within a finite range of carrier density was found in CaB₆(3N) single crystals, but no ferromagnetic signals were detected in CaB₆(6N) single crystals. On the other hand, transport properties of SmB₆ showed that the activation energy and magnetoresistance sign could change depending the Sm vacancies, doping elements, and doping concentration.^[23] Obviously, systematic study of the effects of impurities on the structure of RB₆ including SmB₆ is necessary.

In this article, we report significant differences in the Raman spectra of SmB₆(6N) and SmB₆(3N) and give an explanation based on the impurity-induced structural distortion. All phonon modes in the Raman spectra of SmB₆(3N) strongly shifted to higher wavenumbers and became broader than those of SmB₆(6N) indicating lower symmetry of the crystal structure. However, such lower structure symmetry could not be detected by XRD. Although chemical assay showed that the primary impurities in SmB₆(3N) were Fe ions, the results of our first-principles calculation for the Sm site substituted by Fe ions in SmB₆ could not explain the observed behavior of the Raman spectra. Based on high-pressure experiment and phonon calculation in uniaxial compression model, we proposed that the presence of small amount impurities in SmB₆(3N) is enough to cause spontaneous compression along the [001] axis by ~1%, which could be a consequence of B₆ octahedra tilting away from the [001] direction by about 8°. This mechanism could explain the peculiar behavior in Raman spectra of SmB₆(3N). The unusual dependence of the Raman spectra on impurities reported previously in CaB₆ and EuB₆^[19,20] was similar to our SmB₆ case, implying such common characteristics in the Raman spectra of RB₆ (*R* = Ca, rare earths) could originate from the same mechanism as in SmB₆(3N). Slight structural deformation induced by small amount of impurities might affect the electronic states of SmB₆.

2 | EXPERIMENTAL

2.1 | Sample synthesis

In our experiments, high-quality SmB_6 single crystals were synthesized using the high temperature flux method. A stoichiometric mixture of samarium metal ($\geq 99.9\%$, Alfa Aesar) and boron pieces was placed in an alumina crucible (99.8%, Samhwa Ceramic Company) with aluminum flux (99.999%, RND Korea) at a mass ratio of $\text{SmB}_6:\text{Al} = 1:50$. The $\text{SmB}_6(3\text{N})$ sample was synthesized with 99.9% purity B, whereas the $\text{SmB}_6(6\text{N})$ sample was synthesized with 99.9999% purity B. The mixture was heated in a tube furnace, for which the heating element is MoSi_2 . The heating sequence was started at 300°C to dehydrate the mixture under a high-purity argon atmosphere. After dehydration, the mixture was homogeneously melted at $T = 1,600^\circ\text{C}$ and then slowly cooled to 655°C at a rate of $4.8^\circ\text{C}/\text{hr}$. The synthesized crystals were extracted from the Al flux using NaOH solution. The major impurities in $\text{SmB}_6(3\text{N})$ were Fe (0.0042%) and small amounts of Al (0.00092%), Cr (0.0009%), and Mn (0.0009%).

2.2 | Raman and XRD measurements

Raman spectra were obtained in back-scattering geometry using the XperRam 200 system. A 532.00-nm laser was used as the excitation source, with laser power of ~ 10 mW and beam diameter of ~ 30 μm . XRD patterns of the pulverized single crystals of $\text{SmB}_6(6\text{N})$ and $\text{SmB}_6(3\text{N})$ were obtained at ambient pressure by microfocusing Rigaku D/MAX-2500 with a Cu target radiation wavelength of 1.5406 \AA .

High-pressure Raman and XRD measurements were performed using a Merrill-Bassett-type diamond anvil cell at room temperature. The pressure was recorded using the ruby fluorescence method,^[24] and water was used as the pressure-transmitting media. The high-pressure XRD experiment was performed using MicroMax-007HF (Rigaku Corp.) equipped with rotating anode Mo-K α ($\lambda = 0.7093$ \AA) with multilayer optics (VariMax-Mo, Rigaku) and imaging plate detector (R-axis IV⁺⁺, Rigaku).

3 | RESULTS AND DISCUSSION

3.1 | Differences in Raman spectra of $\text{SmB}_6(6\text{N})$ and $\text{SmB}_6(3\text{N})$

Figure 1a shows the Raman spectra of $\text{SmB}_6(6\text{N})$ and $\text{SmB}_6(3\text{N})$ single crystal samples obtained at 300 K in an unpolarized

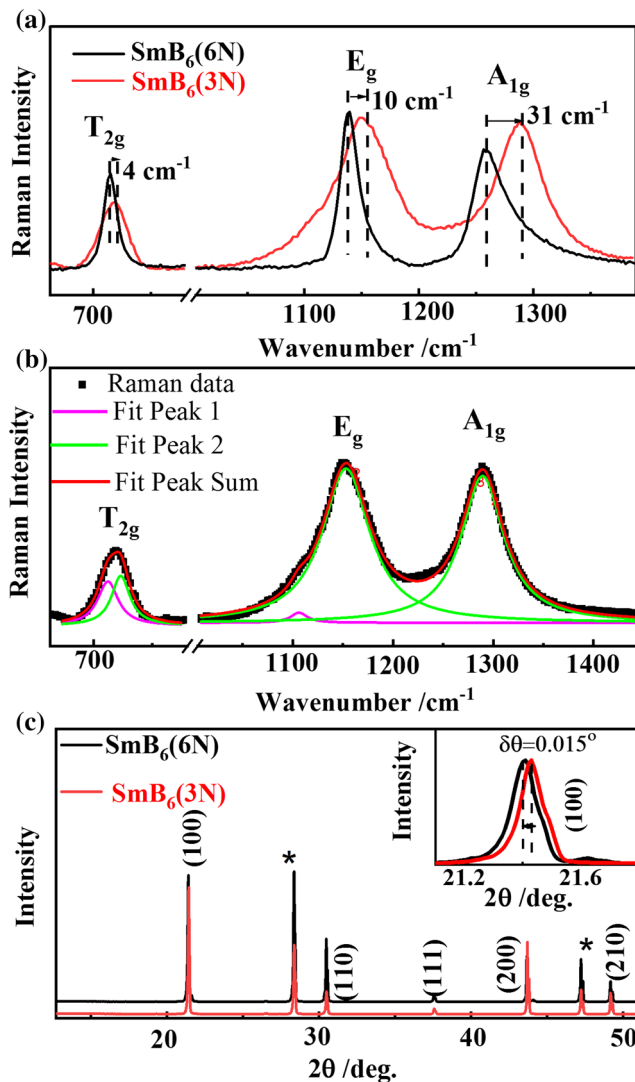


FIGURE 1 (a) Raman spectra of $\text{SmB}_6(6\text{N})$ and $\text{SmB}_6(3\text{N})$ at room temperature show significant differences in Raman shift and linewidth (see the text). The thick black line is for $\text{SmB}_6(6\text{N})$, and the thin red line is for $\text{SmB}_6(3\text{N})$. (b) Doublet features of the T_{2g} and E_g modes of $\text{SmB}_6(3\text{N})$ obtained with Lorentzian fitting. Green and magenta solid lines indicate individual peaks inside each Raman mode, red solid line presents the sum of the fit, and the scattered points are experimental data. Details of the peak positions are listed in Table 1. (c) Powder X-ray diffraction patterns of pulverized single crystals $\text{SmB}_6(6\text{N})$ and $\text{SmB}_6(3\text{N})$. The asterisks indicate silicon peaks which were used for calibration. Inset shows the details of the (100) peak. The difference between $\text{SmB}_6(3\text{N})$ and $\text{SmB}_6(6\text{N})$ is about 0.015° [Colour figure can be viewed at wileyonlinelibrary.com]

configuration. Below $1,400$ cm^{-1} , the Raman spectra of SmB_6 show three phonon modes. These three phonon modes are discerned around 714, 1,139, and $1,259$ cm^{-1} for the 6N sample. These modes are consistent with a factor group analysis, which predicts three Raman-active phonon modes with $T_{2g} + E_g + A_{1g}$ symmetries for the cubic lattice with space group $O_h^1\text{-}Pm\bar{3}m$.^[25] In comparison with

previous reports,^[15–17] the peak at 714 cm⁻¹ can be assigned to T_{2g}, the peak at 1,139 cm⁻¹ to E_g, and the peak at 1,259 cm⁻¹ to A_{1g} mode.

Significant differences in the Raman spectra of SmB₆(6N) and SmB₆(3N) can be clearly observed in Figure 1a; the peaks from the 3N crystal are significantly broader and appear at higher wavenumbers than the corresponding peaks for the 6N crystal. Figure 1b shows the results of fitting the broad peaks of the 3N crystals. The Raman peaks of the 3N crystals shift from those of the 6N crystals by ~4, 10, and 30 cm⁻¹ for the T_{2g}, E_g, and A_{1g} modes, respectively. All of the Raman active modes in SmB₆ are vibrations of B₆ octahedra. The T_{2g} mode is the scissoring displacement of four planar B in the B₆ octahedra. The E_g mode corresponds to a compressing up and down vibration. Both the T_{2g} and E_g modes correspond to modulating B–B–B bond angles. However, the A_{1g} mode is the stretching mode modulating the B–B lengths. Note that B, which has an atomic mass of ~10.81 u, is one of the lightest atoms, and the phonon energies are directly related to the bonding force constants. Therefore, the significant wavenumber increase of the phonon modes in SmB₆(3N) would suggest the following:

1. The major impurities in SmB₆ should go to the Sm sites, not the B sites because the impurities in SmB₆ (Fe, Mn, Al, and so on) are much heavier than B.
2. The bonding force constant in the B₆ octahedra of SmB₆(3N) is larger than that of SmB₆(6N).
3. The stronger upshift of the A_{1g} mode in comparison with the T_{2g} and E_g modes indicates that the change in the force constant related to the B–B bond stretching is larger than that of B–B–B bond angle in the 3N sample.

The possibility of Sm vacancies as the cause of the significant differences between the Raman spectra of SmB₆(6N) and those of SmB₆(3N) can be safely excluded based on previous work by Valentine et al.^[16] They

performed systematic Raman measurements on SmB₆ samples with controlled Sm vacancies. According to their results, Sm vacancies do not affect the peak wavenumbers of the T_{2g}, E_g, and A_{1g} modes at all, though they affect the linewidths slightly.

All the phonon modes of SmB₆(3N) are broader than those of SmB₆(6N). The full widths at the half maximum (FWHM) of Raman peaks of SmB₆(3N) are larger than those in SmB₆(6N) by 15, 33, and 7 cm⁻¹ for the T_{2g}, E_g, and A_{1g}, respectively. The broadening of phonon modes in SmB₆(3N) can be associated with the local disorder^[26] upon introduction of the impurities. However, the T_{2g} and E_g modes of SmB₆(3N) show double peaks compared with the sharp, symmetric single peaks in SmB₆(6N). It is more evident in the Raman spectra of “low-purity Sm¹¹B₆” in supplementary Figure S2. Doublet features of the phonon modes indicate lower symmetry of the crystal structure rather than local disorder. As can be seen in more detail in Figure 1b and Table 1, the T_{2g} and E_g modes in the 3N sample are split into double peaks centered at 712 and 723 cm⁻¹ and 1,107 and 1,153 cm⁻¹, respectively. The ratio of two peaks is approximately 1.015 for the T_{2g} and 1.042 for the E_g mode. Although the ratio of two peaks of the E_g mode is close

to $\sqrt{\frac{^{11}m_B}{^{10}m_B}} = 1.048$, as expected for the B isotopes, we clar-

ify that the double feature of the T_{2g} and E_g modes in SmB₆(3N) is not due to the isotope of ¹⁰B and ¹¹B. We have checked the effects of B isotope on the Raman spectra by synthesizing SmB₆ single crystals with ¹¹B (without any ¹⁰B) with low purity (99.87%) and high purity (99.9999%). The results on the ¹¹B-isotope SmB₆ single crystal samples are presented in detail in Figures S1 and S2. As presented in Figure S1, SmB₆ sample synthesized with ¹¹B with purity 99.87% has the ratio of two peaks of ~1.009 for the T_{2g} and 1.031 for the E_g. So even in the SmB₆ synthesized with ¹¹B only, the doublet feature is still observed when the purity lower than 6N. The A_{1g}

TABLE 1 The Raman active phonon wavenumbers of SmB₆ obtained in experiment and theoretical calculation

SmB ₆	Experiment (cm ⁻¹)			SmB ₆	Theory (cm ⁻¹)		
	T _{2g}	E _g	A _{1g}		T _{2g}	E _g	A _{1g}
ω _{6N}	714 singlet	1,139 singlet	1,259 singlet	Ideal structure (ω _i)	670	1,134	1296
ω _{3N}	712	1,107	1,289	Deformed structure (ω _d)	679	1,143	1,317
	723 doublet	1,153 doublet	singlet		687 doublet	1,161 doublet	Singlet
Splitting/shift ratio	1.54%	4.04%	2.38%	Splitting/shift ratio	1.19%	1.59%	1.62%

Note. The splitting ratio was calculated for the doublet T_{2g} and E_g modes; the amount of splitting between two components of a specific mode of SmB₆(3N) (distorted structure) divided by the wavenumber of the corresponding mode in SmB₆(6N) (ideal structure). The shifting ratio for the singlet A_{1g} mode was calculated with $\frac{(\omega_{3N} - \omega_{6N})}{\omega_{6N}}$ experimentally or $\frac{(\omega_d - \omega_i)}{\omega_i}$ theoretically.

mode in $\text{SmB}_6(3\text{N})$ is also broadened by $\sim 7 \text{ cm}^{-1}$, and random disorder^[26] may also explain it. But aforementioned random disorder may not explain the doublet features in T_{2g} and E_g modes. In our density functional theory (DFT) calculation for the A_{1g} mode, we could get only a single peak shift but no doublet feature. However, lower symmetry in the SmB_6 crystal structure can explain the broadening of the A_{1g} mode as well.

Local symmetry breaking in $\text{SmB}_6(3\text{N})$ is proposed to account for the presence of extra Raman peaks than the factor group analysis prediction within the cubic symmetry. However, in contrast to the behavior in Raman spectra, the XRD patterns of $\text{SmB}_6(6\text{N})$ and $\text{SmB}_6(3\text{N})$ show no forbidden or additional peaks (see Figure 1c). The diffraction angle of the (100) peak shows a shift of $\sim 0.015^\circ$ (inset of Figure 1c). Likewise, the (110) peak shows a shift of $\sim 0.011^\circ$, and the peak (111) shows identical behavior (figure not shown), indicating no significant difference in lattice parameter of two samples. Indeed, the values of the lattice parameters are obtained to be 4.13371(3) and 4.13293(2) Å for the $\text{SmB}_6(6\text{N})$ and $\text{SmB}_6(3\text{N})$, respectively. They are close to each other and in agreement with previous publications.^[19,20,27] Thus, XRD does not show any clear evidence of lower crystal symmetry in $\text{SmB}_6(3\text{N})$. However, our Raman results suggest that the local environment of the B_6 octahedra is distorted leading to local symmetry breaking.

Before going to explain the peculiar behavior in Raman spectra of $\text{SmB}_6(3\text{N})$, we emphasize that the similar dependence of Raman spectra on impurities was also observed in other hexaboride RB_6 compounds. For instance, strong effects of impurities in the B ingredients were reported in the Raman study of $\text{CaB}_6(6\text{N})$ and $\text{CaB}_6(3\text{N})$ single crystals.^[19] In our previous Raman research, all the phonon modes of $\text{CaB}_6(3\text{N})$ were found

to be broader and shifted to higher wavenumbers compared with those of $\text{CaB}_6(6\text{N})$. The E_g mode of $\text{CaB}_6(3\text{N})$, in particular, showed doublet feature. Similar phonon peak broadening and upshifts were also found in $\text{Eu}_{1-x}\text{La}_x\text{B}_6$ ($x = 0, 0.05, 0.1, 0.2,$ and 0.3) synthesized with 99.9999% purity B.^[20] It seems to be a general phenomenon that small amount of impurities introduces lower symmetry in RB_6 , for $R = \text{Ca}, \text{Eu},$ and Sm at least. Finding a common mechanism which describes effect of impurity on local structural symmetry in RB_6 is necessary.

3.2 | High-pressure Raman and XRD of $\text{SmB}_6(6\text{N})$

In order to correlate the effect of impurity to structural distortion in $\text{SmB}_6(3\text{N})$, XRD patterns and the Raman spectra of $\text{SmB}_6(6\text{N})$ crystal were investigated at various pressures. The pressure dependence of the XRD patterns and Raman spectra and the lattice compression of $\text{SmB}_6(6\text{N})$ are shown in Figure 2a–c, which confirm that there is no structural phase transition up to 3.0 GPa. The lattice constant a for the cubic phase is found to be continuously decreasing with increasing pressure (Figure 2c). The values of a are 4.14569(5) and 4.11712(6) Å at pressures of 0.0 and 3.0 GPa, respectively. The reduction in the lattice constant a is about 0.7% with the application of 3.0-GPa pressure.

We quantitatively analyzed the pressure dependence of the Raman spectra of $\text{SmB}_6(6\text{N})$. As can be seen in Figure 2d, the FWHM values of the Raman phonons are not significantly affected by the pressure. This is in contrast to the broad Raman peaks observed in $\text{SmB}_6(3\text{N})$ crystals. In our high-pressure experiments in a diamond anvil cell, a quasi-hydrostatic condition was

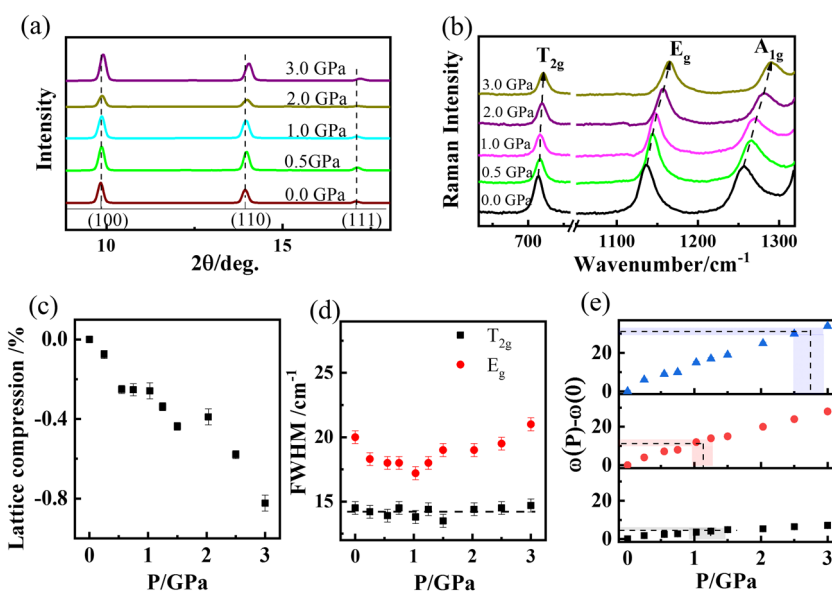


FIGURE 2 Pressure (0.0–3.0 GPa) dependence of the (a) X-ray diffraction patterns, (b) Raman spectra, (c) lattice compression, (d) full widths at the half maximum of T_{2g} (black squares) and E_g (red circles) modes, and (e) relative shifts in wavenumber of the T_{2g} (black squares), E_g (red circles), and A_{1g} (blue triangles) Raman modes of $\text{SmB}_6(6\text{N})$ single crystal [Colour figure can be viewed at wileyonlinelibrary.com]

maintained up to ~ 1.5 GPa where the water pressure-transmitting media froze to ice VI so that the structural symmetry of the $\text{SmB}_6(6\text{N})$ crystal was kept below 1.5 GPa. Consequently, the FWHM of the phonon modes was barely affected up to 1.5 GPa. However, the broader T_{2g} , E_g , and A_{1g} phonon modes of the 3N crystal compared with those of the 6N crystal suggest that the symmetry of the structure is lower in $\text{SmB}_6(3\text{N})$. We speculate that the lower symmetry of $\text{SmB}_6(3\text{N})$ might be due to anisotropic distortion in the B_6 octahedra as described below.

The relationship of the relative peak shift ($\omega_{(P)} - \omega_{(0)}$) and pressure is plotted in Figure 2e. All the T_{2g} , E_g , and A_{1g} phonon modes shift to higher wavenumbers with increasing pressure, and the E_g and A_{1g} phonons show a slightly faster upshift than the T_{2g} mode. Similar behavior is observed in the phonon modes of $\text{SmB}_6(3\text{N})$ at ambient pressure in comparison with those of $\text{SmB}_6(6\text{N})$. The wavenumbers for the T_{2g} and E_g modes of the 6N crystal reach the same values as the corresponding modes of the $\text{SmB}_6(3\text{N})$ crystal at ~ 1.5 GPa, whereas the pressure value for the A_{1g} mode reach ~ 2.5 to 3.0 GPa. In Figure 2e, the horizontal dashed line for each mode indicates the experimental wavenumber difference for $\text{SmB}_6(3\text{N})$ with respect to the corresponding mode of $\text{SmB}_6(6\text{N})$ at ambient pressures. Then, the vertical line for each mode can be regarded as the “virtual pressure” that may exist in $\text{SmB}_6(3\text{N})$. Higher virtual pressure for the A_{1g} mode is consistent with the fact that the A_{1g} vibrational eigenvector is the largest along the c -direction, which implies that the deformation in $\text{SmB}_6(3\text{N})$ is anisotropic. This interpretation suggests that the reduction along the c -direction could occur in $\text{SmB}_6(3\text{N})$.

A natural question arises regarding the main cause for the broadening and strong upshifts of the phonon modes. The Fano resonance was observed in the A_{1g} mode in $\text{SmB}_6(6\text{N})$ in contrast to symmetric shape in $\text{SmB}_6(3\text{N})$, which suggests coherent interference between the discrete phonon and a broad peak or continuum, that is, the electron–phonon coupling in $\text{SmB}_6(6\text{N})$.^[28] Typically, the Fano peak is described by Breit–Wigner function

$$I(\omega) = A \frac{[q + \varepsilon(\omega)]^2}{1 + \varepsilon(\omega)^2}, \quad \varepsilon(\omega) = \frac{2(\omega - \omega_0)}{\Gamma},$$

where ω_0 is the phonon frequency, A is the amplitude, q is the asymmetric parameter, and Γ describes the resonance width. Interestingly, the electron–phonon coupling would lower the wavenumber of a phonon mode. So the recovery of Fano shape and upshift of the A_{1g} mode in $\text{SmB}_6(3\text{N})$ could be associated with electron–phonon coupling by introduction of impurities. It is worth to note that the Fano shape was found in the A_{1g} mode of $\text{CaB}_6(3\text{N})$ with higher

wavenumber compared with symmetric A_{1g} mode in $\text{CaB}_6(6\text{N})$.^[19] It is clear that the electron–phonon coupling may explain the Fano-shape but not the upshift of the phonon mode in SmB_6 as well as CaB_6 at the same time. Thus, the upshift of the phonon modes in 3N sample may not be related electron–phonon coupling in RB_6 ($R = \text{Ca}, \text{Eu}, \text{and Sm}$). Extra free charge carriers generated by the impurities in $\text{CaB}_6(3\text{N})$ were suggested by Rhyee et al.^[21] as a possible source for the renormalization of the phonon self-energies, though without a theoretical support. To better understand the broadening and upshift of the phonon modes, we conducted a systematic theoretical investigation as following.

3.3 | Phonon wavenumber calculation by the first-principles DFT

The phonon wavenumbers in the ideal structure (perfect cubic symmetry) for RB_6 ($R = \text{Sc}, \text{Fe}, \text{Y}, \text{Mg}, \text{Sm}, \text{Ca}, \text{and Sr}$) were calculated by using the first-principles DFT. We used Perdew–Bruke–Ernzerhof-type generalized gradient approximation^[29] to DFT and the project augmented-wave method, as implemented in the Vienna Ab initio Simulation Package.^[30] We used the experimental lattice parameter for SmB_6 and calculated relaxed atomic positions inside the unit cell by minimizing the total energy. For the other compounds, the lattice parameters and atomic positions were obtained by minimizing the total energy. An energy cutoff of 1,000 eV was used for the plane-wave expansion, and $10 \times 10 \times 10$ Monkhorst–Pack k-point grid was used for the Brillouin-zone integration. The spin–orbit interaction was included for SmB_6 . We calculated the interatomic

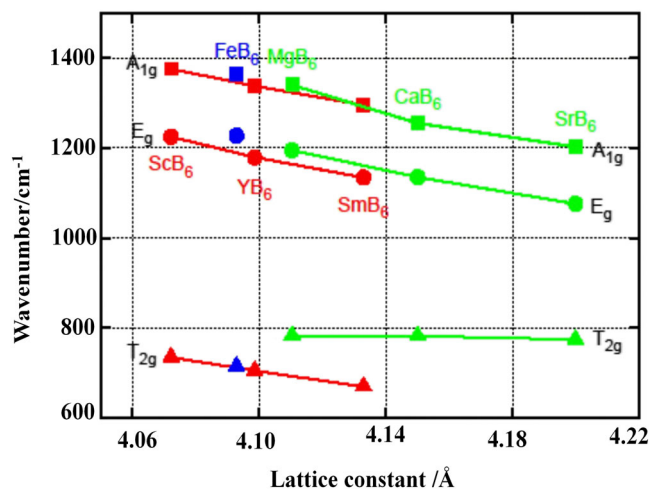


FIGURE 3 Relation between phonon wavenumber (cm^{-1}) and lattice parameter in several RB_6 hexaboride compounds calculated with density functional theory [Colour figure can be viewed at wileyonlinelibrary.com]

force constant matrices using the density functional perturbation theory^[31] and obtained the wavenumbers of the Raman active phonon modes from the interatomic force constant matrices.

The general trend of the calculated phonon wavenumbers shown in Figure 3 are in good agreement with the experimental findings by Ogita et al.^[17] Note that all the phonon modes of FeB₆ have higher wavenumbers than the corresponding modes of SmB₆. Thus, the upshifts of the Raman modes of SmB₆(3N) could have been explained by doping the Sm site with Fe, which is the major impurity in the 3N boron used in synthesizing the SmB₆(3N). However, at most, 0.1% of Sm would be replaced by Fe in SmB₆(3N), so that the major portion of the SmB₆ would show Raman modes at the original (lower) wavenumbers and the minor component at higher wavenumbers. Experimentally, the Raman spectra of SmB₆(3N) in Figure 1b show that the T_{2g} and E_g Raman modes consist of multiple peaks and the major (minor) components of the Raman modes are at higher (lower) wavenumbers, contrary to our theoretical expectations for doping of the Sm site with Fe impurities.

Even if the Raman modes are affected by Fe doping, the amount of Raman peak shifts would not be as large as the difference in the wavenumbers of the corresponding Raman modes of FeB₆ and SmB₆. To the contrary, our experimental findings show that upshifts of the Raman modes are quite large for only 0.1% of impurities.

In order to explain the discrepancy, we need to assume anisotropic deformation of the cubic SmB₆ structure. The phonon wavenumbers are first calculated in perfect cubic symmetry and later with the assumption of a 1% reduction only along the [001] axis. First, for the ideal structure, we used experimental lattice parameters for SmB₆ $a = 4.133 \text{ \AA}$ ^[27] and calculated relaxed atomic positions inside the unit cell by minimizing the total energy until residual

forces on the atoms are smaller than 0.001 eV/Å. After relaxation, one Sm atom is at (0, 0, 0) and six B atoms are at $(a/2, a/2, \pm 0.1995a)$, $(a/2, \pm 0.1995a, a/2)$, and $(\pm 0.1995a, a/2, a/2)$. Subsequently, for comparison with the SmB₆(3N) samples, the symmetry of the atomic structure is lowered by reducing the lattice constant c along the z axis by 1% from the experimental value, and the lattice constants a and b along the other two axes are fixed, that is, $a = b$ and $c = 0.99a$. With this uniaxial deformation, atomic positions inside the unit cell are relaxed again by minimizing the total energy. After relaxation, one Sm atom is at (0, 0, 0) and six B atoms are at $(a/2, a/2, \pm 0.1994c)$, $(a/2, \pm 0.1994a, c/2)$, and $(\pm 0.1994a, a/2, c/2)$. Figure 4 shows the theoretical Raman spectra of the ideal and 1% compressed structure. The details of the phonon wavenumbers from the experimental (for 6N and 3N crystals) and calculations (for the ideal and deformed structure) are listed in Table 1.

As can be seen in Figure 4 and Table 1, the behaviors of the deformed structure significantly resemble the behaviors of the 3N sample.

1. The wavenumbers of all the phonon modes show upshifts from the ideal to deformed structure. This is consistent with the experimental fact that phonon wavenumbers of SmB₆(3N) are higher than those of SmB₆(6N).
2. The relative ratio of the shifted wavenumbers of the phonon modes of SmB₆(3N) with respect to those of SmB₆(6N) is comparable with the theoretical values calculated assuming ~1% compression along the c axis.
3. Doublet features of the T_{2g} and E_g modes are in agreement with the double components obtained by fitting the Raman spectra of SmB₆(3N) (Figure 1b) and by two dimensional correlation spectroscopy and principal component analysis (2DCOS+PCA).^[32]

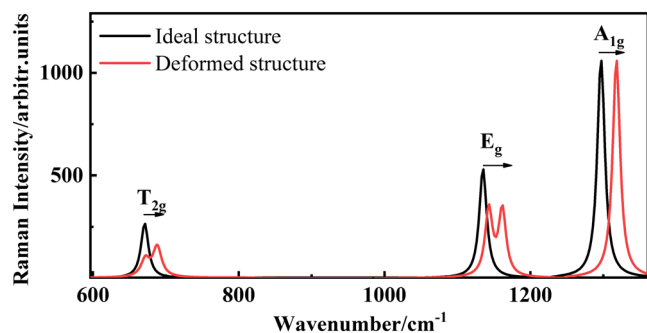


FIGURE 4 Density functional theory calculation of the phonon wavenumbers of SmB₆ in the anisotropic compression model. The black solid line represents the ideal structure (without any distortion), and the red solid line represents the deformed structure, in which the lattice parameter is reduced by 1% along the c axis [Colour figure can be viewed at wileyonlinelibrary.com]

These results imply that our model with a slightly uniaxial compression is a good assumption to explain the shifting and broadening (multiple-peak feature) of the Raman spectra of SmB₆(3N). The consistent results in theoretical calculation and high-pressure Raman spectroscopy revealed that compression by 1% of the lattice parameter along the c axis is an appropriate hypothesis to explain the peculiar behaviors observed in the Raman spectra of the 3N sample. Note that the tetragonal symmetry induced by breaking the cubic symmetry reported in EuB₆^[33] (B purity 99.99%) is consistent with our interpretation in this point of view. However, the origin of tetragonal distortion was not explained in the previous case. Our analyses above indicate the impurities played an important role in inducing local structural distortion in SmB₆(3N) or even in RB₆ compounds. This leads to

the question of how such a deformation could occur in RB_6 octahedral structure in reality, and we suggest spontaneous tilting or rotation of the B_6 octahedra in $SmB_6(3N)$ as one of a possibilities.

3.4 | Distortion of B_6 octahedron assumption

Tilting/rotation of octahedral BX_6 is a very common structural distortion in perovskite materials. The best known example of a perovskite with tilted octahedra is $SrTiO_3$. A phase transition from the ideal cubic structure to a tetragonal structure occurs at ~ 105 K due to the tilting/rotation of the octahedron TiO_6 away from the c axis.^[34–36] However, if octahedron tilting from the $[001]$ axis causes a structural phase transition, the unit cell should be expanded twice along the $[100]$ and $[010]$ directions as well. In $SmB_6(3N)$, no evidence of a structural phase transition or doubling of the lattice constant could be found in XRD pattern. However, we still propose that the B_6 octahedra may be *slightly* tilted away from the $[001]$ direction in $SmB_6(3N)$. If the unit cell is compressed 1% along the $[001]$ direction as in our theoretical model, then the titled angle is estimated to be about 0.141 (rad) or $\sim 8.1^\circ$ as schematically illustrated in Figure 5a. From the macroscopic perspective, imagine that each B_6 cage is titled with a small angle in any unit cell, then another B_6 cage in the next unit cell is also titled a little but in the opposite direction to the

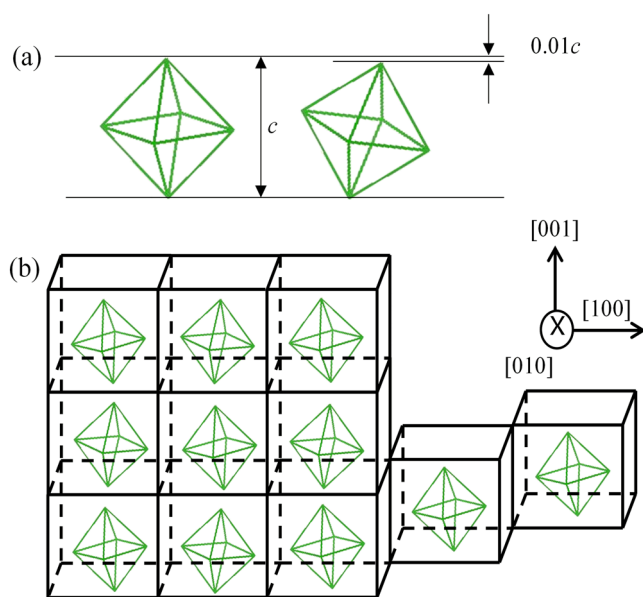


FIGURE 5 (a) Schematic illustrations of the B_6 octahedron in ideal and distorted cases (slightly tilted away from the $[001]$ direction). (b) Proposed arrangement of tilted B_6 octahedra in unit cells. Every B_6 cage tilts in the opposite direction with respect to the next B_6 cage [Colour figure can be viewed at wileyonlinelibrary.com]

original distortion (Figure 5b). The tilting can extend several unit cells and form a small domain size. The orientation of each domain can be random. As a result, the average macroscopic structure of SmB_6 is not affected at all. The tilting of the B_6 cage in SmB_6 is a reasonable scenario because of the following advantages:

1. It preserves the degeneracy of a, b axis.
2. It maintains the inversion symmetry.
3. It explains a “natural” compression along c axis.

The most important thing is, in this model, the tilting/rotation of the B_6 cage by a small angle may not be detectable with XRD or neutron scattering due to two reasons. First, ^{149}Sm and ^{10}B ions are strong neutron absorbers, and the electron clouds of the B_6 cage (along c axis in perfect crystal) still retain a nearly spherical shape when it is distorted slightly. Second, according to Thomson's^[37] equation, the XRD intensity of an atom is proportional to the number of electrons,

$$I \propto \frac{ZI_0}{r} \left[\frac{e^2}{m_e c^2} \right]^2 \frac{1 + \cos^2(2\theta)}{2}$$

where Z is number of electrons, I_0 is intensity of incident beam, r is distance from electron to detector, $\frac{e^2}{m_e c^2}$ is the classical electron radius, 2θ is angle

between scattering and incident beam. In our case, the octahedron B_6 in RB_6 is formed by light B atoms ($Z = 5$); therefore, the tilting/rotation of octahedron is hard to detect using XRD. It is in contrast to the case of octahedral MX_6 in perovskites, which both center (M cation) and surround X_6 cage are much heavier than B ion. This may explain the fact that all XRD studies of $CaB_6(3N)$,^[19] $Eu_{1-x}La_xB_6$,^[20] $EuB_6(99.99\% \text{ B purity})$,^[33] and $SmB_6(3N)$ could not recognize the possible tetragonal distortion in crystal structure. Tilting of the B_6 octahedra is one plausible scenario that can occur in the RB_6 ($R = \text{rare-earth element}$) structure, and we suggest that such tilting/rotation of the B_6 octahedra is triggered by the presence of small amount ($\sim 0.1\%$ at most) of impurities.

3.5 | Structural distortion and physical properties of RB_6

Having the impurity-induced structural distortion scenario, we comment on the relation of the impurity in B ingredients to their physical properties of RB_6 . It was pointed out that difference in B purity leads to difference in electronic and magnetic properties of CaB_6 in previous reports.^[21,22] They suggested that the defect from impurities generate the local magnetic moment and extra free carriers in $CaB_6(3N)$ compounds, which could not be found in $CaB_6(6N)$. Even with different stoichiometric $CaB_{6-\delta}(3N)$, $CaB_{6+\delta}(3N)$ or small none

magnetic ions La-doping $\text{Ca}_{0.995}\text{La}_{0.005}\text{B}_6(3\text{N})$ also showed FM signals, whereas none of corresponding 6N samples revealed FM order. In EuB_6 , the cubic symmetry prevents the occurrence of FM phase; however, it is reported that the FM order in low purity EuB_6 exists below 16 K.^[38] A tetragonal symmetry induced from cubic symmetry breaking was assumed to explain the FM behavior.^[33] Note that the B purity in Martinho et al.^[33] is 4N (99.99%), lower than 6N (99.9999%), which was our highest B purity for $\text{SmB}_6(6\text{N})$ or $\text{CaB}_6(6\text{N})$. Therefore, our impurity-induced structural distortion scenario seems to be applicable to their interpretation as well. In SmB_6 , due to lack of single crystal quality information, especially impurity ingredients in B sources in previous literatures which reported about the intriguing but contradictory properties of SmB_6 , we cannot compare the effects of impurities directly with their findings such as 2-D nature or 3-D nature of electronic states. However, several groups used different methods with different purity of ingredients in synthesizing their samples. For instance, Hatnean et al.^[39] produced crystals by floating zone from commercial SmB_6 powder (99.9%), reporting 3-D conduction electron Fermi state.^[8] Jiang et al.^[14] grew single crystal by Al-flux method from a chunk of Sm (99.9%) and B powder (99.99%) and argued wide range of surface state up to 150 K. They all used low purity than 99.9999% (6N) ingredients in the sample synthesis.

We claim that the structural distortion caused by presence of impurities can affect electronic states of SmB_6 . Indeed, it is well known that the nontrivial state of SmB_6 is related to conduction state on the surfaces and formation of small gap inside which results from the hybridization of localized *f*-electrons and itinerant *d*-electrons of Sm ions. First, according to recent theoretical calculation,^[40] the wave function at X point has the contribution from the B_6 cluster suggesting another hybridization of 4*f*-bands of Sm with 2*p*-states of B. Thus, the deformation/tilting of B_6 octahedron could affect such hybridization leading to changes in the electronic properties of SmB_6 . Second, the Fano-shape of the A_{1g} mode was also observed in an independent Raman study by Robinson et al.^[41] on pure SmB_6 (0% ^{10}B), in agreement with our results. They pointed out its origin from interaction of phonon and interband excitation electronic back grounds of Sm bands. In our study, the asymmetric factor *q* of the A_{1g} mode is ~ 4.4 and 2.2×10^{23} (i.e., Lorentzian shape) for the $\text{SmB}_6(6\text{N})$ and $\text{SmB}_6(3\text{N})$, respectively. Clearly, the impurities do affect the electronic structure of SmB_6 and changes the electron-phonon coupling as seen in different line shapes of the A_{1g} mode of 3N and 6N. We suggest that some of the peculiar physical properties of SmB_6

reported previously could be related with the B ingredient purity. Further detailed study of the relationship between the physical properties and purity of the ingredients is opened for future task.

We believe that impurity-induced distortion in $\text{SmB}_6(3\text{N})$ is a common effect which could happen in RB_6 compounds, at least for $R = \text{Ca}, \text{Eu},$ and Sm . It is noted that the major impurities in RB_6 ($R = \text{Ca}, \text{Eu},$ and Sm) are all different elements. They can be a light element (C as in CaB_6) or heavier ions (La in EuB_6 and Fe in SmB_6). However, no matter what the major impurity was, strong Raman shift to higher wavenumber and line broadening (doublet feature) are found all in $\text{SmB}_6(3\text{N})$, $\text{CaB}_6(3\text{N})$, and La-doped EuB_6 . The presence of impurities seems to trigger the B_6 octahedron distortion, affecting the electronic state, and lead to impurity dependence of some physical properties in these compounds. From our interpretation, such local structural distortion in RB_6 would show clear signatures in Raman spectra, but it is hard to detect using other conventional techniques such as XRD or neutron scattering. Our study demonstrates Raman scattering as a simple and powerful method to investigate microscopic structural distortion in RB_6 .

4 | CONCLUSION

In summary, microscopic changes in the structure of impurity-controlled SmB_6 were investigated using Raman spectroscopy and first-principles calculations. The Raman spectra of $\text{SmB}_6(3\text{N})$ and $\text{SmB}_6(6\text{N})$ exhibited significant differences in wavenumber and line shape in contrast to essentially identical behavior in XRD patterns. We suggest that the presence of $\sim 0.1\%$ (at most) of impurities in $\text{SmB}_6(3\text{N})$ induces a slight B_6 octahedra distortion, such as spontaneous tilting away from the [001] direction, leading to significant upshifts of the phonon peak wavenumbers and broadening of the phonon modes of $\text{SmB}_6(3\text{N})$ in comparison with those of $\text{SmB}_6(6\text{N})$, the purest sample. The impurity-induced structural distortion in $\text{SmB}_6(3\text{N})$ could be a common effect in RB_6 including CaB_6 and EuB_6 , leading to varieties of physical properties. This work exemplifies the strength of Raman spectroscopy to study the change in the microscopic structure of materials composed of light element such as RB_6 .

ACKNOWLEDGEMENTS

I. S. Y. acknowledges the support by the National Research Foundation of Korea (NRF) grant funded by the Korean Ministry of Science and ICT (2017R1A2B2009309). B. Y.

K. and B. K. C. acknowledges the support by the NRF of Korea (Grant NRF-2017R1A2B2008538). M. H. and H. J. C. acknowledge support from the NRF of Korea (Grant 2011-0018306). Computational resources were provided by KISTI Supercomputing Center (Project KSC-2016-C3-0006). Y.L. is grateful for the NRF-2018R1A3B1052042 grant from the Korean Ministry of Science and ICT.

ORCID

In-Sang Yang  <https://orcid.org/0000-0003-4956-2197>

REFERENCES

- [1] R. L. Cohen, M. Eibschütz, K. W. West, *Phys. Rev. Lett.* **1970**, 24, 383.
- [2] J. C. Cooley, M. C. Aronson, Z. Fisk, P. C. Canfield, *Phys. Rev. Lett.* **1995**, 74, 1629.
- [3] A. Barla, J. Derr, J. P. Sanchez, B. Salce, G. Lapertot, B. P. Doyle, R. Rüffer, R. Lengsdorf, M. M. Abd-Elmeguid, J. Flouquet, *Phys. Rev. Lett.* **2005**, 94, 166401.
- [4] E. Frantzeskakis, N. de Jong, B. Zwartsenberg, Y. K. Huang, Y. Pan, X. Zhang, J. X. Zhang, F. X. Zhang, L. H. Bao, O. Tegus, A. Varykhalov, A. de Visser, M. S. Golden, *Phys. Rev. X* **2013**, 3, 041024.
- [5] M. Dzero, K. Sun, V. Galitski, P. Coleman, *Phys. Rev. Lett.* **2010**, 104, 106408.
- [6] M. Dzero, K. Sun, P. Coleman, V. Galitski, *Phys. Rev. B* **2012**, 85, 045130.
- [7] G. Li, Z. Xiang, F. Yu, T. Asaba, B. Lawson, P. Cai, C. Tinsman, A. Berkley, S. Wolgast, Y. S. Eo, D.-J. Kim, C. Kurdak, J. W. Allen, K. Sun, X. H. Chen, Y. Y. Wang, Z. Fisk, L. Li, *Science* **2014**, 346, 1208.
- [8] B. S. Tan, Y.-T. Hsu, B. Zeng, M. Ciomaga Hatnean, Z. Z. N. Harrison, M. Hartstein, M. Kiourlappou, A. Srivastava, M. D. Johannes, T. P. Murphy, J.-H. Park, L. Balicas, G. G. Lonzarich, G. Balakrishnan, S. E. Sebastian, *Science* **2015**, 349, 287.
- [9] M. Neupane, N. Alidoust, S. Y. Xu, T. Kondo, Y. Ishida, D. J. Kim, C. Liu, I. Belopolski, Y. J. Jo, T. R. Chang, H. T. Jeng, T. Durakiewicz, L. Balicas, H. Lin, A. Bansil, S. Shin, Z. Fisk, M. Z. Hasan, *Nat. Commun.* **2013**, 4, 2991.
- [10] N. J. Laurita, C. M. Morris, S. M. Koohpayeh, P. F. S. Rosa, W. A. Phelan, Z. Fisk, T. M. McQueen, N. P. Armitage, *Phys. Rev. B* **2016**, 94, 165154.
- [11] P. K. Biswas, M. Legner, G. Balakrishnan, M. C. Hatnean, M. R. Lees, D. M. Paul, E. Pomjakushina, T. Prokscha, A. Suter, T. Neupert, Z. Salman, *Phys. Rev. B* **2017**, 95, 020410(R)
- [12] M. Hartstein, W. H. Toews, Y. T. Hsu, B. Zeng, X. Chen, M. C. Hatnean, Q. R. Zhang, S. Nakamura, A. S. Padgett, G. Rodway-Gant, J. Berk, M. K. Kingston, G. H. Zhang, M. K. Chan, S. Yamashita, T. Sakakibara, Y. Takano, J. H. Park, L. Balicas, N. Harrison, N. Shitsevalova, G. Balakrishnan, G. G. Lonzarich, R. W. Hill, M. Sutherland, S. E. Sebastian, *Nat. Phys.* **2017**, 14, 166.
- [13] N. Xu, C. E. Matt, E. Pomjakushina, X. Shi, R. S. Dhaka, N. C. Plumb, M. Radovic, P. K. Biswas, D. Evtushinsky, V. Zabolotnyy, J. H. Dil, K. Conder, J. Mesot, H. Ding, M. Shi, *Phys. Rev. B* **2014**, 90, 085148.
- [14] J. Jiang, S. Li, T. Zhang, Z. Sun, F. Chen, Z. R. Ye, M. Xu, Q. Q. Ge, S. Y. Tan, X. H. Niu, M. Xia, B. P. Xie, Y. F. Li, X. H. Chen, H. H. Wen, D. L. Feng, *Nat. Commun.* **2013**, 4, 3010.
- [15] P. Nyhus, S. L. Cooper, Z. Fisk, J. Sarrao, *Phys. Rev. B* **1995**, 52, R14308.
- [16] M. E. Valentine, S. Koohpayeh, W. A. Phelan, T. M. McQueen, P. F. S. Rosa, Z. Fisk, N. Drichko, *Phys. Rev. B* **2016**, 94, 075102.
- [17] N. Ogita, S. Nagai, N. Okamoto, M. Udagawa, F. Iga, M. Sera, J. Akimitsu, S. Kunii, *Phys. Rev. B* **2003**, 68, 224305.
- [18] N. Ogita, S. Nagai, N. Okamoto, F. Iga, S. Kunii, T. Akamtsu, J. Akimitsu, M. Udagawa, *J. Solid State Chem.* **2004**, 177, 461.
- [19] M. Song, I.-S. Yang, J. Y. Kim, B. K. Cho, *Vib. Spectrosc.* **2006**, 42, 288.
- [20] M. Song, I.-S. Yang, C. W. Seo, H. Cheong, J. Y. Kim, B. K. Cho, *J. Mag. Mag. Mater.* **2007**, 310, 1019.
- [21] J.-S. Rhyee, B. K. Cho, *J. Appl. Phys.* **2004**, 95, 6675.
- [22] B. K. Cho, J.-S. Rhyee, B. H. Oh, M. H. Jung, H. C. Kim, Y. K. Yoon, J. H. Kim, T. Ekino, *Phys. Rev. B* **2004**, 69, 113202.
- [23] S. Gabáni, M. Orendáč, G. Pristáš, E. Gažo, P. Diko, S. Piovarči, V. Glushkov, N. Sluchanko, A. Levchenko, N. Shitsevalova, K. Flachbart, *Philos. Mag.* **2016**, 96, 3274.
- [24] H. K. Mao, J. Xu, P. M. Bell, *J. Geophys. Res.* **1986**, 91, 4673.
- [25] R. Loudon, *Adv. Phys.* **1964**, 13, 423.
- [26] R. Shuker, R. W. Gammon, *Phys. Rev. Lett.* **1970**, 25, 222.
- [27] S. Rossler, T. H. Jang, D. J. Kim, L. H. Tjeng, Z. Fisk, F. Steglich, S. Wirth, *Proc. Natl. Acad. Sci.* **2014**, 111, 4798.
- [28] U. Fano, *Phys. Rev.* **1961**, 124, 1866.
- [29] J. P. Perdew, K. Burke, M. Ernzerhof, *Phys. Rev. Lett.* **1996**, 77, 3865.
- [30] G. Kresse, J. Furthmüller, *Phys. Rev. B* **1996**, 54, 11169.
- [31] S. Baroni, S. de Gironcoli, A. Dal Corso, P. Giannozzi, *Rev. Mod. Phys.* **2001**, 73, 515.
- [32] T. H. Nguyen, T. M. H. Nguyen, B. Kang, B. Cho, Y. Park, Y. M. Jung, I.-S. Yang, *J. Mol. Struct.* **2018**, 1165, 84.
- [33] H. Martinho, C. Rettori, G. M. Dalpian, J. L. da Silva, Z. Fisk, S. B. Oseroff, *J. Phys. Condens. Matter* **2009**, 21, 456007.
- [34] H. Unoki, T. Sakudo, *J. Physical Soc. Japan* **1967**, 23, 546.
- [35] P. A. Fleury, J. F. Scott, J. M. Worlock, *Phys. Rev. Lett.* **1968**, 21, 16.
- [36] A. D. Bruce, R. A. Cowley, *Structural Phase Transition*, Vol. 34, Taylor and Francis, London **1981** 58.
- [37] J. J. Thomson, *Conduction of Electricity through Gases*, Cambridge Univ, Press **1906**.
- [38] S. Paschen, D. Pushin, M. Schatter, P. Vonlanthen, H. R. Ott, D. P. Young, Z. Fisk, *Phys. Rev. B* **2000**, 61, 4174.
- [39] M. C. Hatnean, M. R. Lees, D. M. Paul, G. Balakrishnan, *Sci. Rep.* **2013**, 3, 3071.
- [40] C.-J. Kang, J. Kim, K. Kim, J. Kang, J. D. Denlinger, B. I. Min, *J. Physical Soc. Japan* **2015**, 84, 024722.

- [41] P. J. Robinson, M. E. Valentine, A. Granmoe, N. Drichko, J. R. Chamorro, P. F. Rosa, T. M. McQueen, A. N. Alexandrova, **2019**; arXiv:1903.10650

SUPPORTING INFORMATION

Additional supporting information may be found online in the Supporting Information section at the end of the article.

How to cite this article: Nguyen TH, Nguyen TMH, Kang B, et al. Raman spectroscopic evidence of impurity-induced structural distortion in SmB₆. *J Raman Spectrosc.* 2019;50:1661–1671. <https://doi.org/10.1002/jrs.5709>